Supplementary material

Drivers of aerosol variability in the high Arctic: insights from integrated observations at Gruvebadet and Zeppelin (Ny-Ålesund)

Elena Barbaro[1], Francisco Ardini[2], Silvia Becagli[3], Stefano Bertinetti[4], Federica Bruschi[6], Giulia Calzolai[5], Alice Cavaliere[1], David Cappelletti[6,1], Stefano Crocchianti[6], Matteo Feltracco[7,8,1], Andrea Gambaro[7,1], Fabio Giardi[5], Stefania Gilardoni[1], Marco Grotti[2], Dominic Heslin-Rees[8], Radovan Krejci[8], Mery Malandrino[4], Matilde Mataloni[2], Simonetta Montaguti[9], Silvia Nava[10,5], Marco Paglione[9], Matteo Rinaldi[9], Chiara Ripa[1], Mirko Severi[3], Andrea Spolaor[1], Rita Traversi[3], Hilde Uggerud[11], Giulio Verazzo[1], Tessa Viglezio[1], Karl Espen Yttri[11], Wenche Aas[11], Mauro Mazzola[1].

S1.1 Meteorological and radiation data

Key meteorological variables, such as air temperature, relative humidity, atmospheric pressure, wind speed and direction, and stability parameters (Fig. S1), but also solar (shortwave) radiation, net longwave radiation and surface albedo were evaluated (Fig. S2). Daily values are shown with time series, while the wind rose and histogram for stability parameters were generated with 30- minute averages.

Daily temperatures fluctuated between -25°C and +25°C, staying below zero from winter to spring and rising in summer. Wind speeds mostly remained under 10 m s^{-1}, with a dominant E-SW pattern aligned with Kongsfjorden. Notably, Mazzola et al. (2016) observed similar statistical distributions for wind components during summer.The stability parameter z/L shifted from positive (stable) to negative (unstable) values during summer, a behavior strictly linked to snow-free ground between June and October (Becherini et al., 2021). Snow cover increases albedo and limits heating, promoting stability, while snow-free soil enhances solar absorption and vertical mixing. Figure S1c confirms that >50% of Obukhov length values are positive.Radiative data showed solar peaks exceeding 350 W m^{-2} in spring/summer, dropping to zero during the polar night. Net longwave flux remained mostly negative, indicating winter radiative cooling, though clouds or inversions caused occasional positive shifts. Surface albedo decreased from 0.9 (snow-covered) to below 0.3 in summer as tundra or water became exposed.

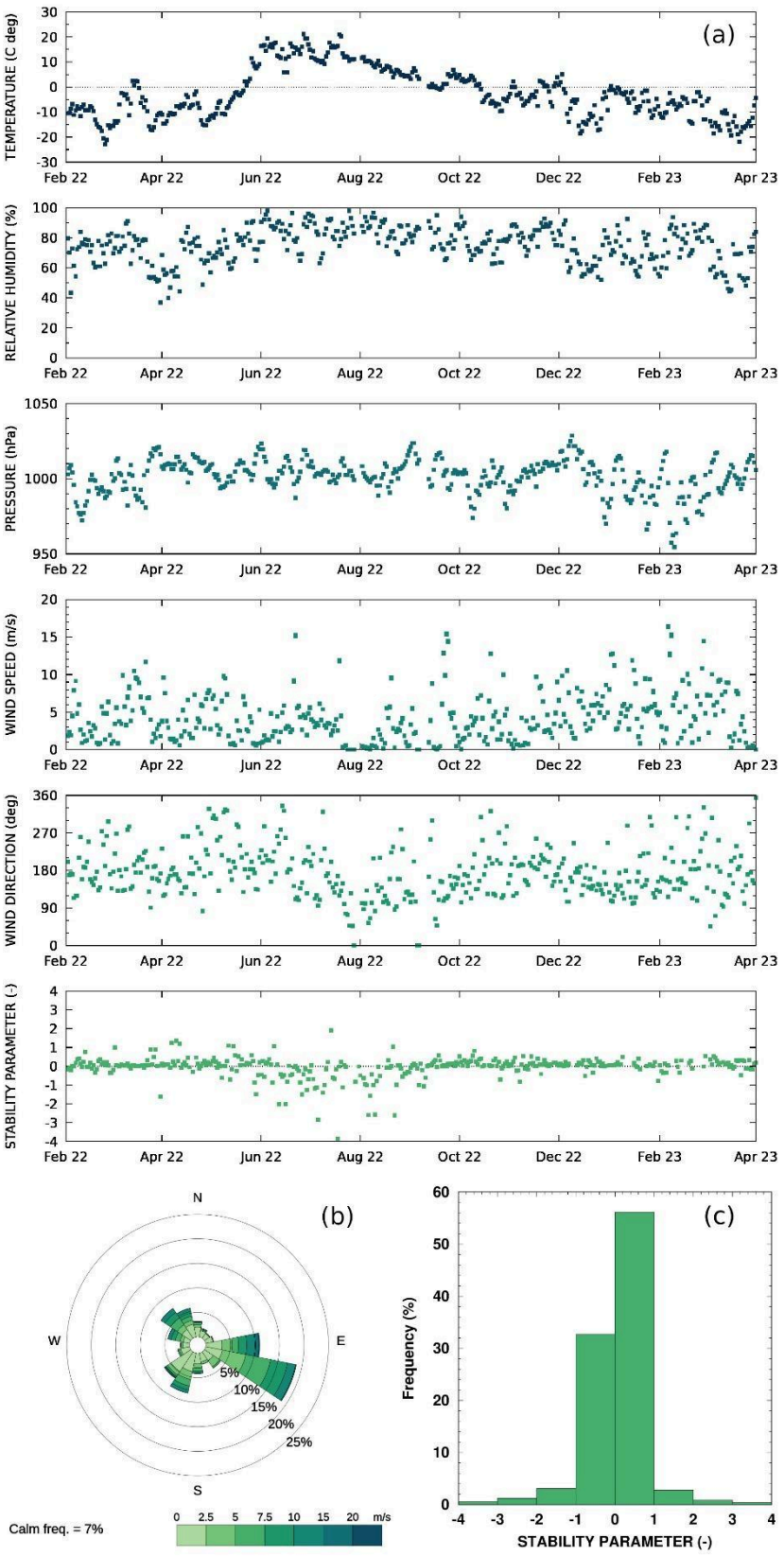

Figure S1. (a) Time series of daily values of meteorological and stability parameters measured at CCT during the study period. (b) Polar plot of the wind patterns. (c) Frequency histogram of the stability parameter. Plots in (b) and (c) were obtained using 30-minute values.

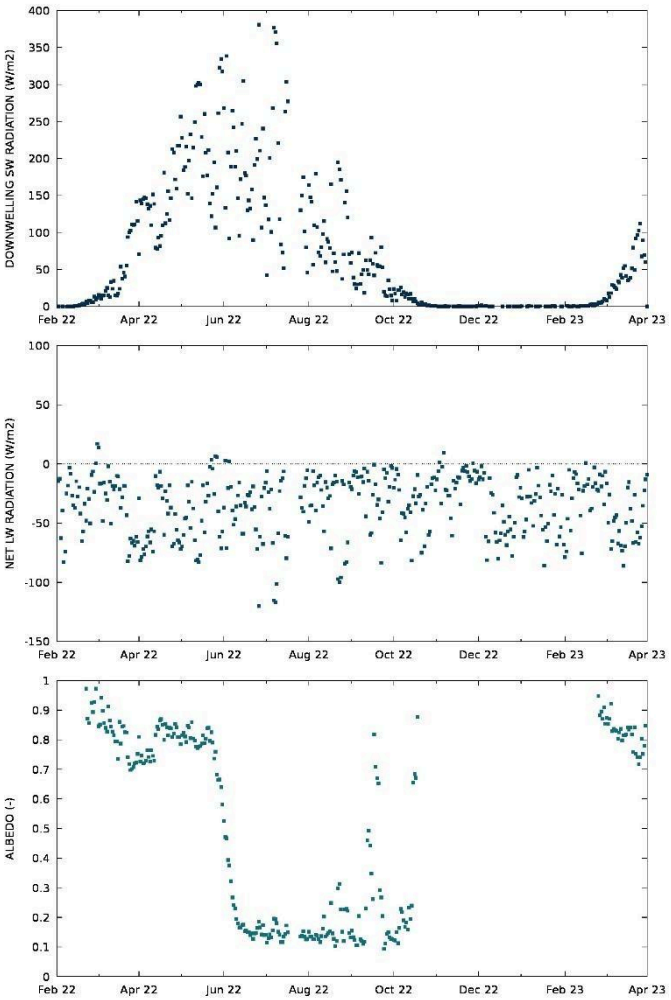

Figure S2. Time series of daily values of solar radiation (upper panel), net longwave radiation (middle panel) and surface albedo (lower panel) measured at CCT during the study period.

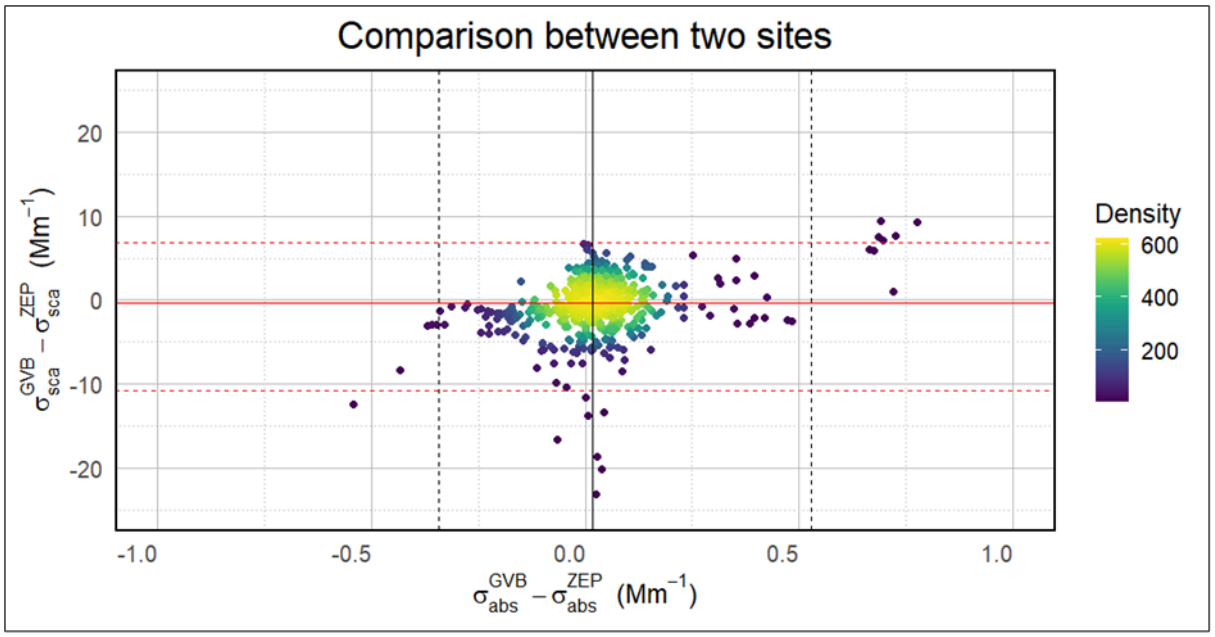

Figure S3. Scatterplot between the difference of hourly σ_{abs} (at the two sites) and the difference of σ_{sca} (at the two sites). The horizontal axis represents the difference in absorption coefficients between GVB and ZEP, while the vertical axis shows the

difference in scattering coefficients. The solid line denotes the median for each variable, whereas the dashed lines indicate the 1st and 99th percentiles. This plot applied the Bland-Altman representation to datasets characterized by a non-normal distribution (Shapiro-Wilk test: p-value < 2.2×10^{-16}).

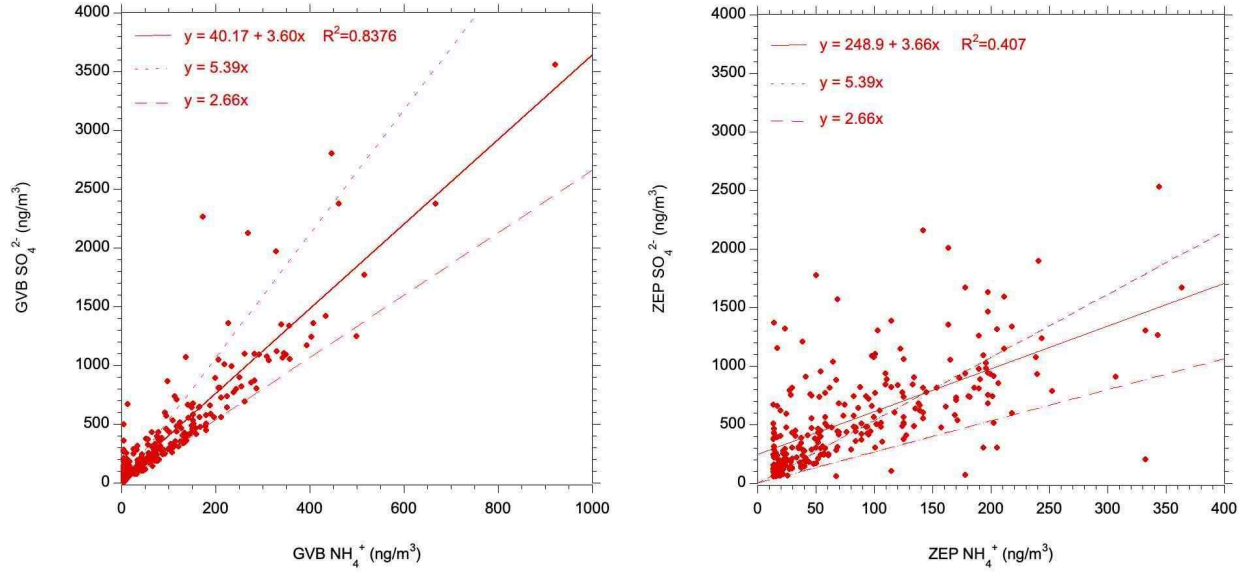

Figure S4. Linear correlation between sulphate and ammonium obtained using the entire dataset from Jan 2022 to Jun 2023 at GAL and ZEP.

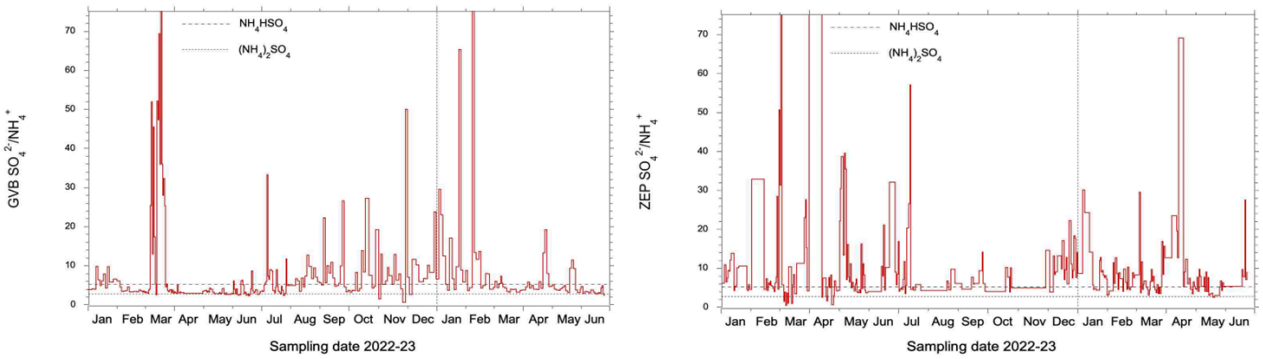

Figure S5. SO_4^{2-}/NH_4^+ ratio (w/w) obtained from the dataset from Jan 2022 to Jun 2023 at GAL and ZEP.

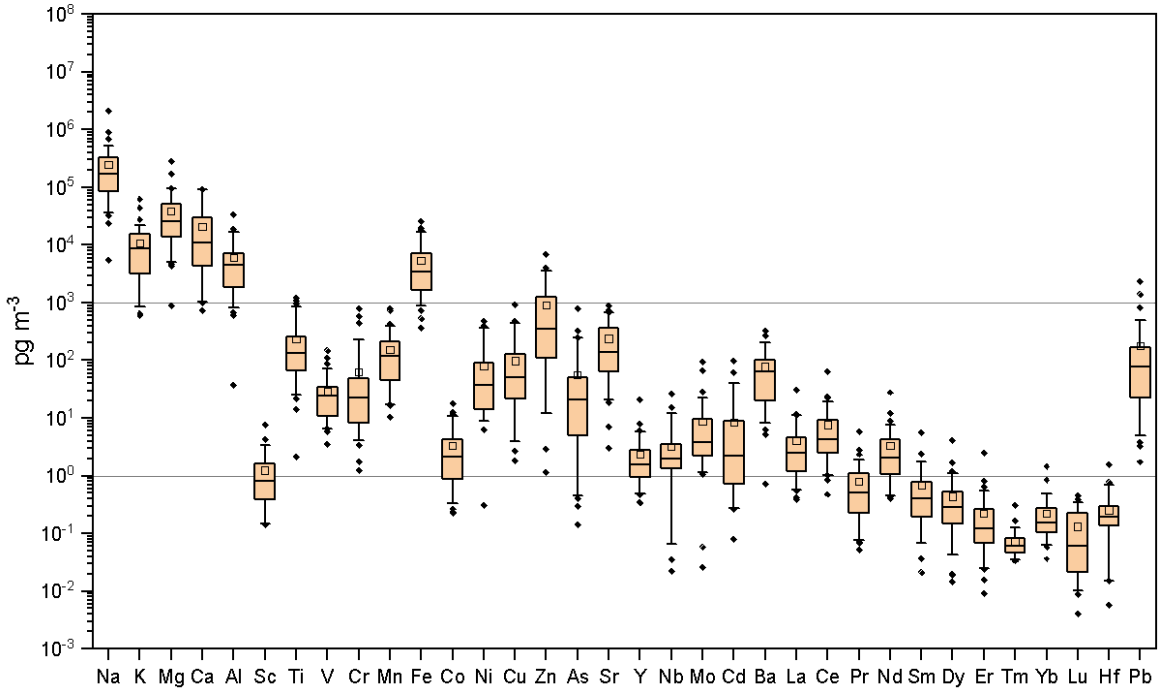

Figure S6. Boxplot for the mass concentration in air of the elements monitored in the PM_{10} samples. The extremes of the whiskers point to the 5th and 95th percentile of each distribution.

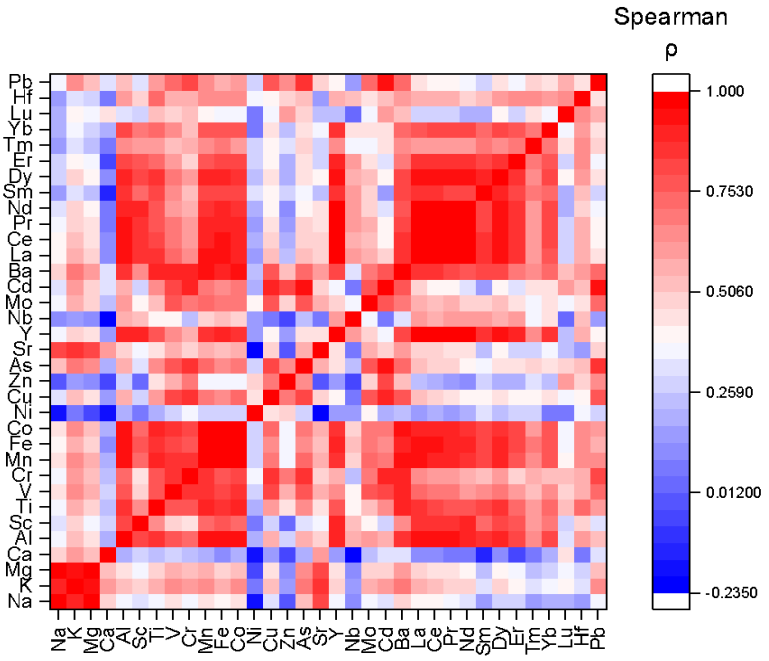

Figure S7. Spearman's ρ correlation coefficient for the concentration of the elements normalized for the relative maximum value.

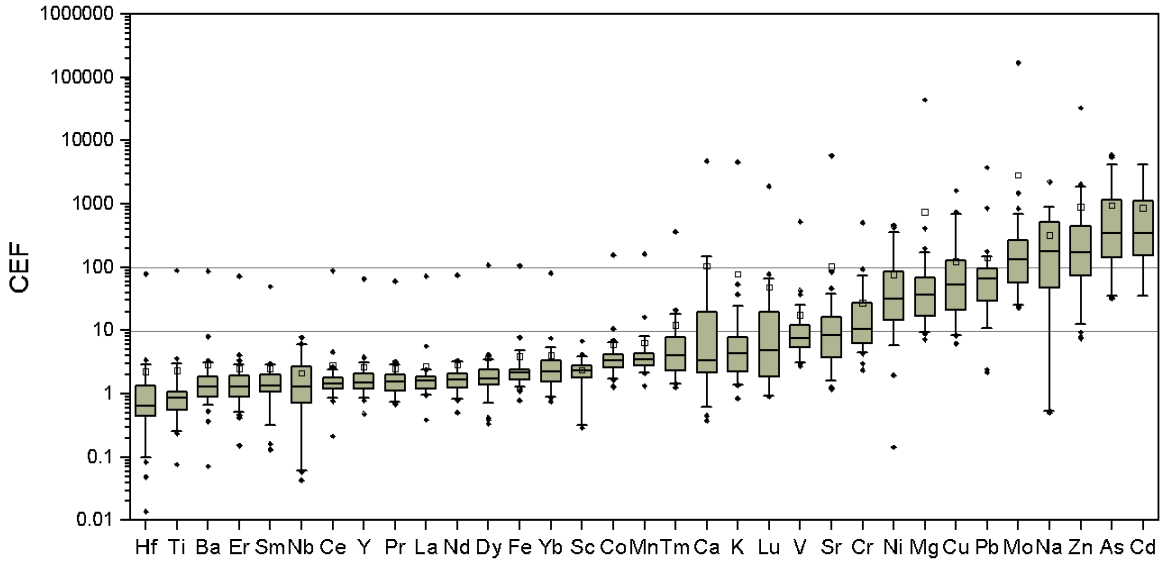

Figure S8. Boxplot for the crustal enrichment factors. The elements are sorted by increasing median order. The extremes of the whiskers point the 5th and 95th percentile of each distribution.

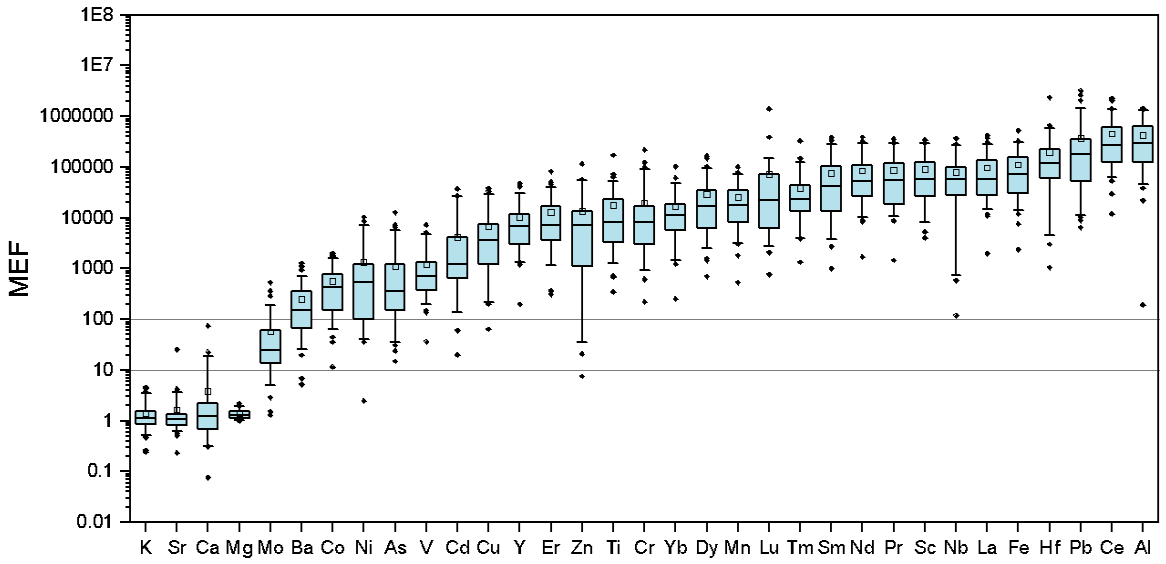

Figure S9. Boxplot for the marine enrichment factors. The elements are sorted by increasing median order. The extremes of the whiskers point the 5th and 95th percentile of each distribution.

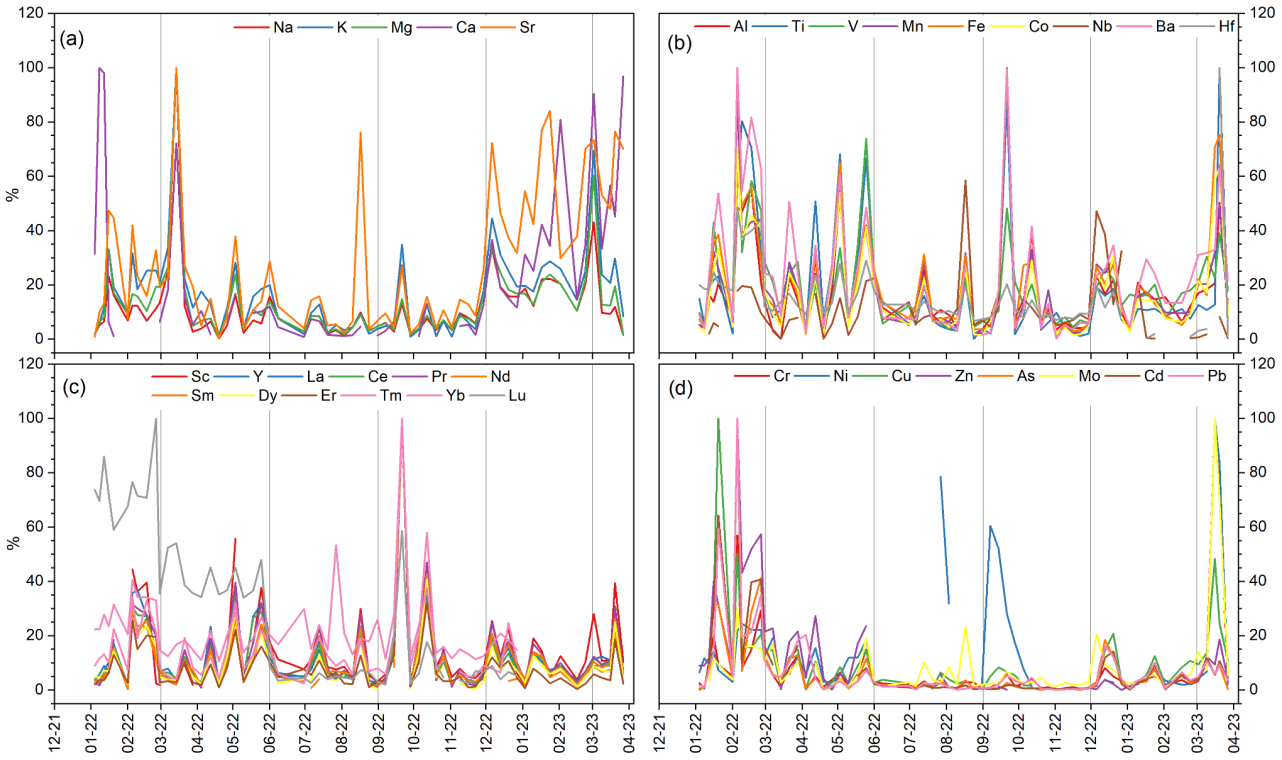

Figure S10. Temporal trend of the elemental concentration normalized with respect to the maximum value. The elements are grouped according to their value of CEF and MEF, which define the specific sources: a) marine, b) and c) crustal, and d) anthropogenic sources.

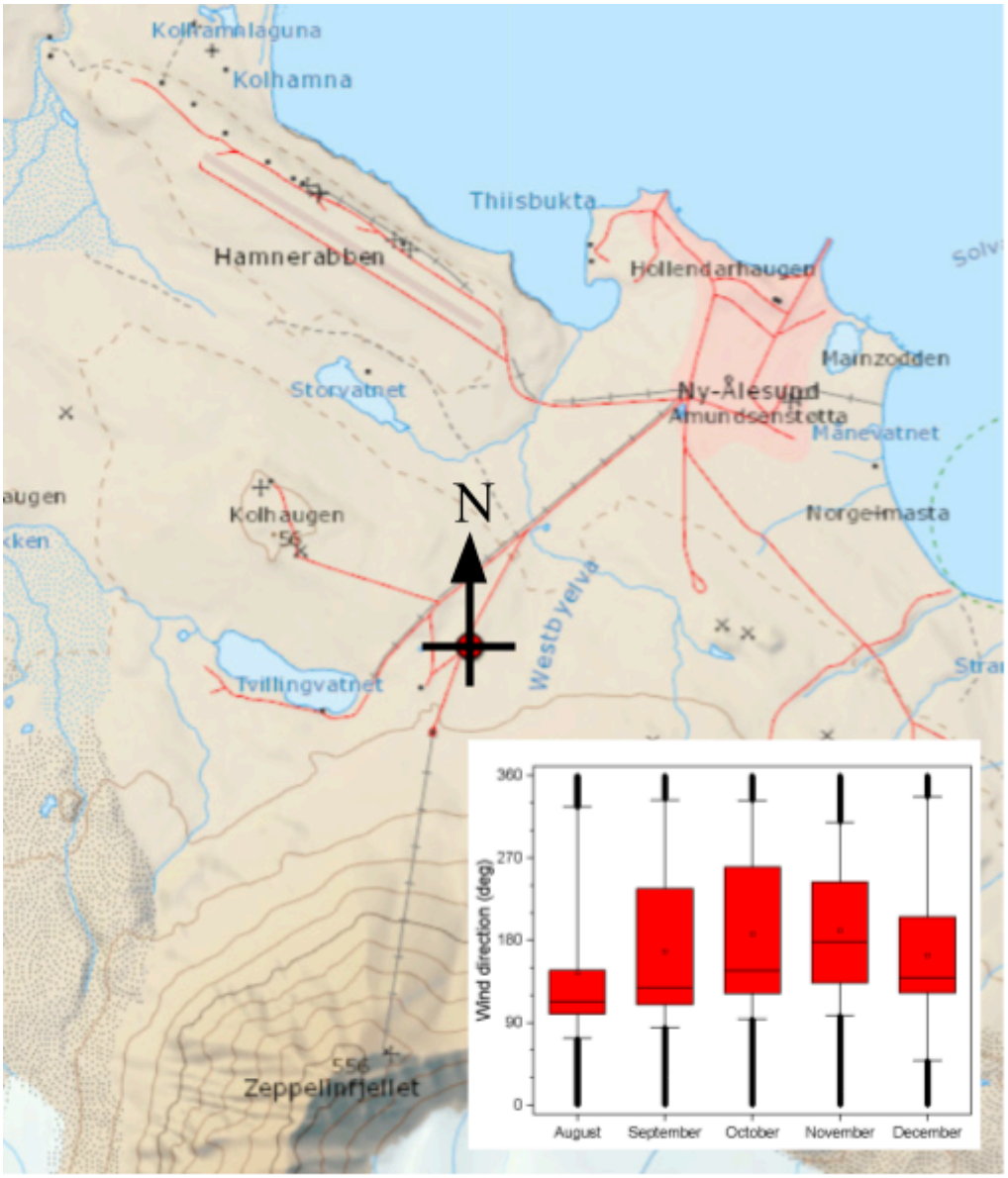

Figure S11. Map of Ny-Ålesund and surrounding area with the indication of the Gruvebadet atmospheric laboratory (red point). In the insert, the wind direction recorded from August to December 2022 is shown as boxplot. The extremes of the whiskers point to the 5th and 95th percentile of each distribution.

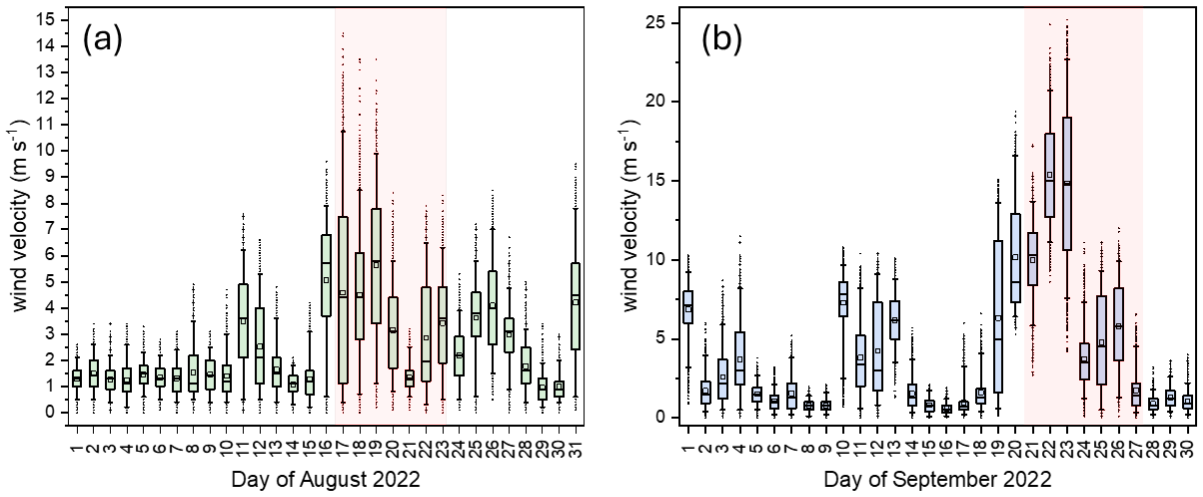

Figure S12. Boxplot for the wind velocity for each day of August and September 2022. The extremes of the whiskers point the 5th and 95th percentile of each distribution.

Table S1. Summary of the results for Pb concentration, isotope ratio values, and crustal enrichment factors (CEFs) for PM_{10} samples collected at GAL from February 2022 to March 2023 (n = 58).

Statistics	Pb (pg/m^3)	CEF	$^{208}Pb/^{206}Pb$	$^{207}Pb/^{206}Pb$
Mean	174	127	2.102	0.861
SD	287	157	0.010	0.005
Min	4.4	5.9	2.073	0.848
Q1	21	35	2.096	0.859
Median	80	69	2.103	0.861
Q3	191	149	2.108	0.863
Max	1823	778	2.119	0.874
IQR	170	114	0.012	0.004

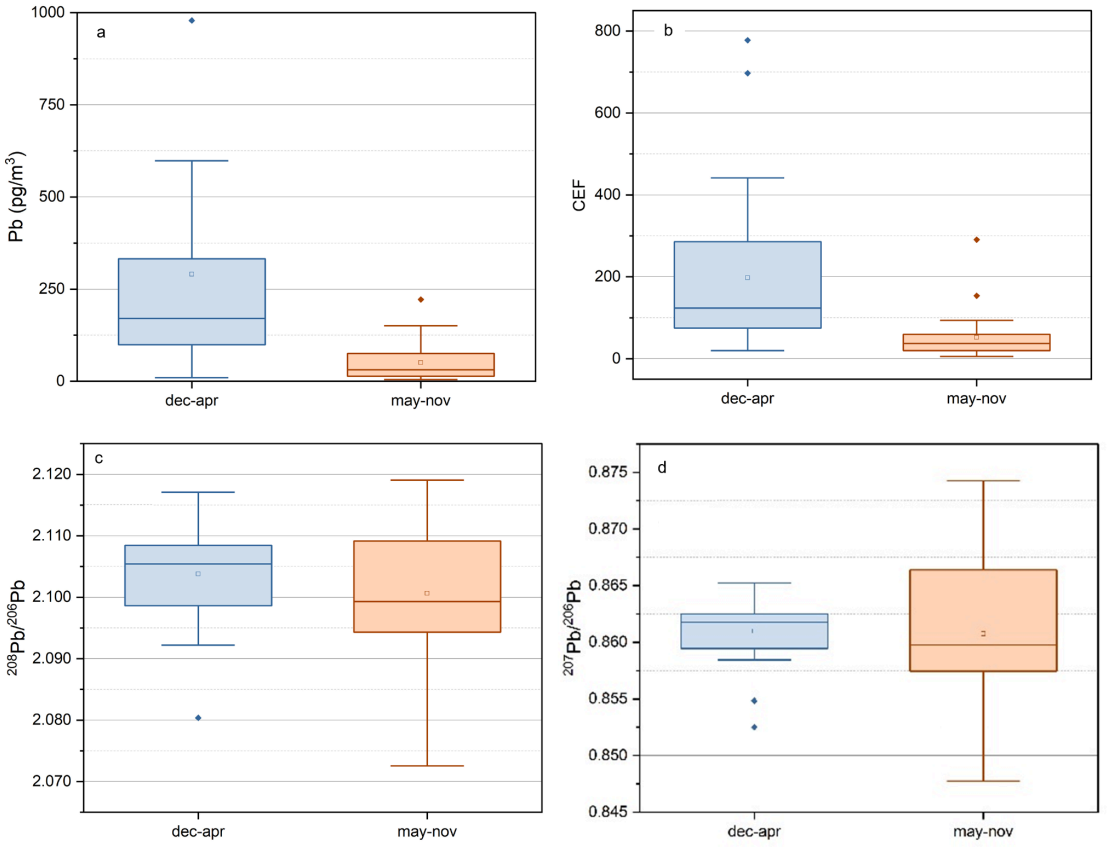

Fig. S13. Boxplot representation of Pb data. a) Pb concentration, b) CEF, c) $^{208}Pb/^{206}Pb$ and d) $^{207}Pb/^{206}Pb$. Each box is delimited by 25^{th} and ^{75}th percentiles; thick line represents the median, whiskers indicate the minimum and maximum values within 1.5 interquartile range, and dots are values outside the whiskers (outliers).

Fig. S14. Enrichment factor of silicon**.**

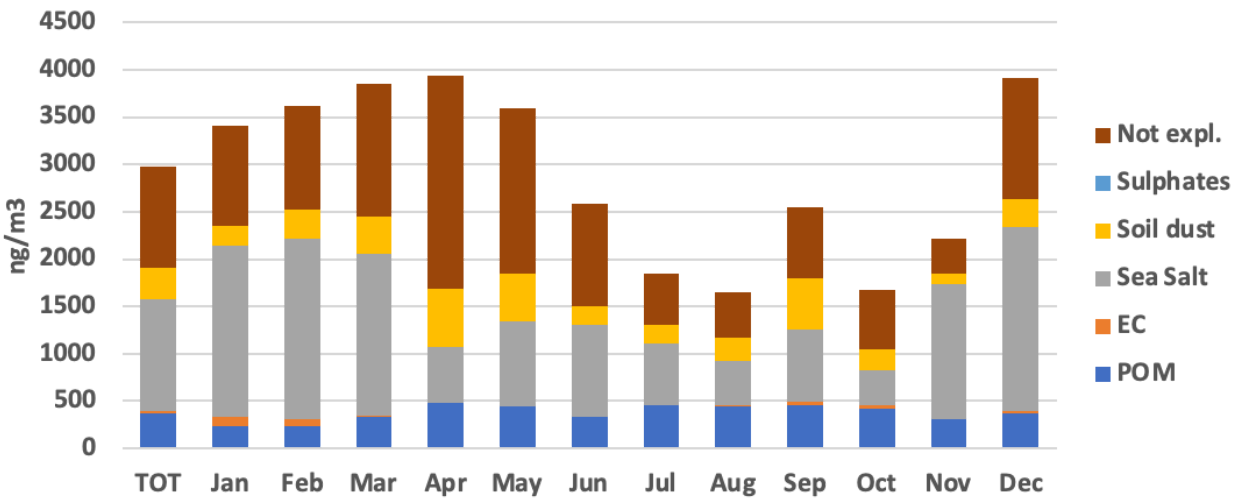

Fig. S15. Monthly average aerosol mass.

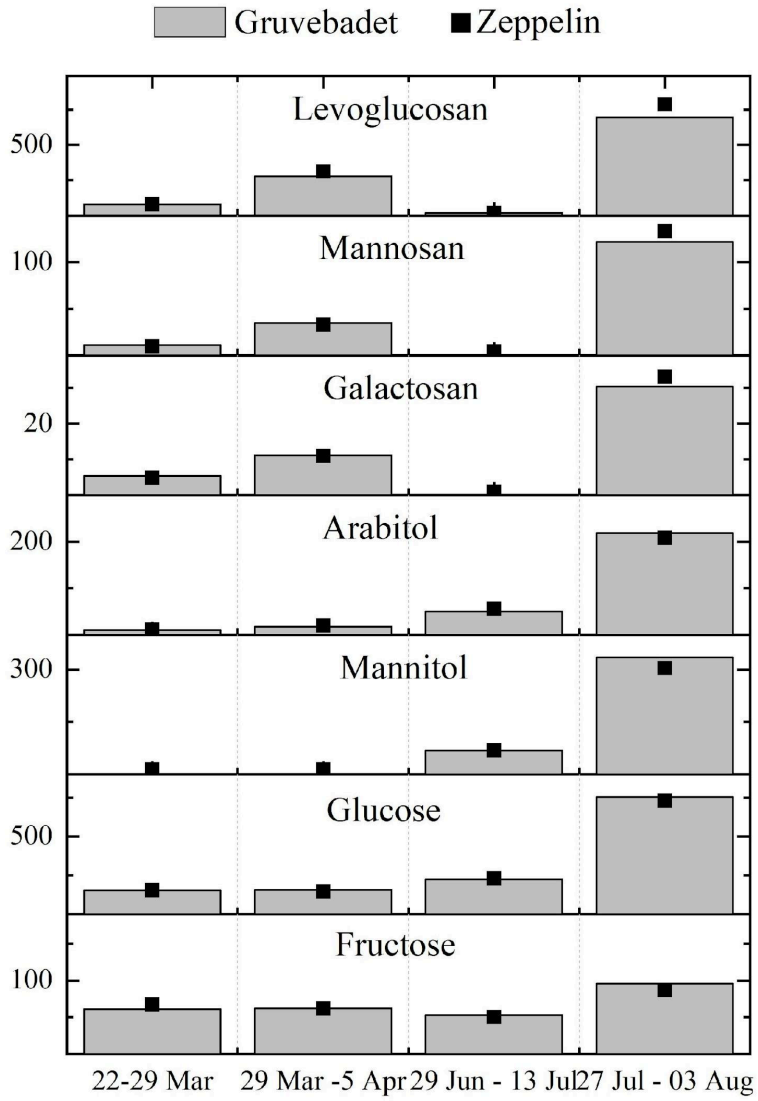

Figure S16: Intercomparison exercise in which the Venice Lab quantified the same samples collected at ZEP using its own method. The results were also determined by NILU for comparison.

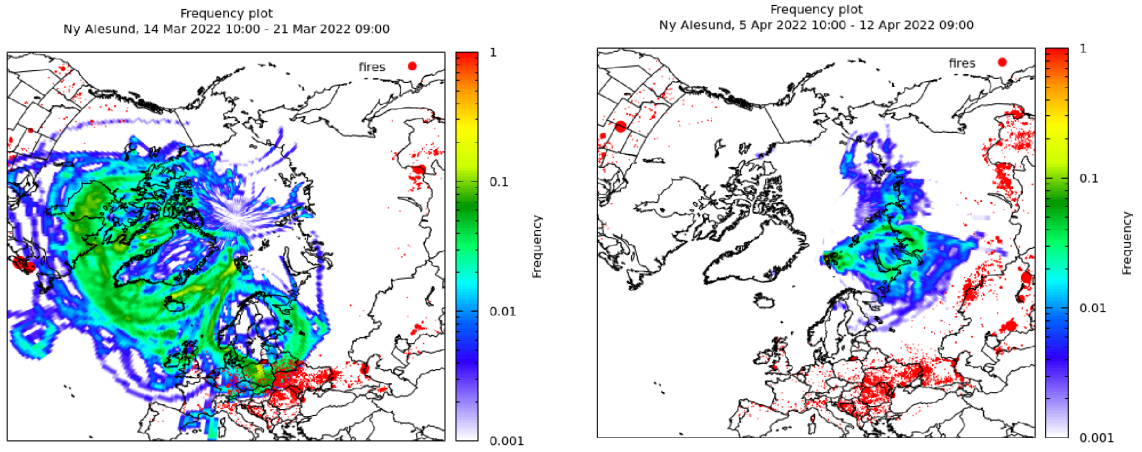

Figure S17: Frequency plot (note the logarithmic scale) for trajectories reaching the site from 10:00 of Mar 14 to 9:00 of Mar 21, 2022 (left hand side panel) and from 10:00 of 5 Apr to 9:00 12 Apr 2022 (right hand side panel). Fires from Modis are represented as red circles whose diameter is proportional to the fire radiative power.

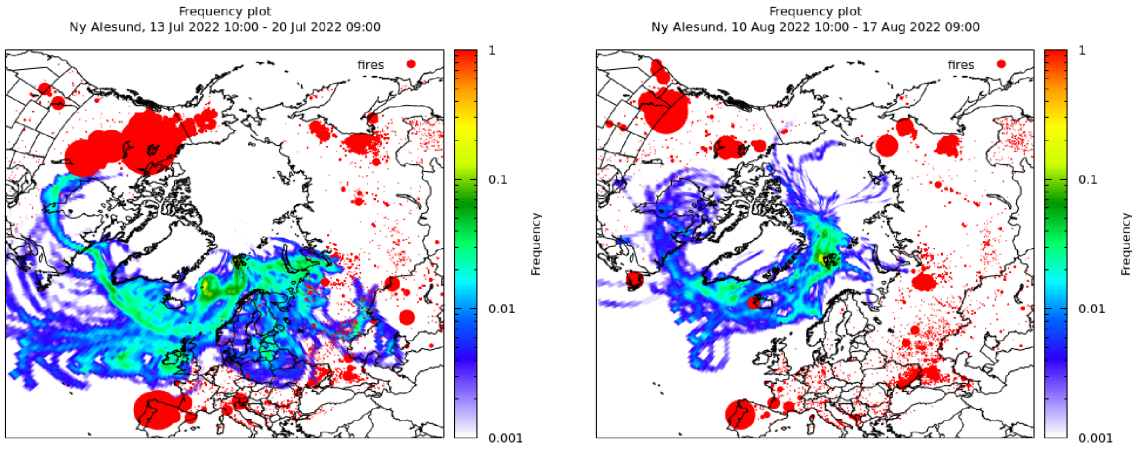

Figure S18: Frequency plot (note the logarithmic scale) for trajectories reaching the site from 10:00 of Jul 13 to 9:00 of Jul 20, 2022 (left hand side panel) and from 10:00 of 10 Aug to 9:00 17 Aug 2022 (right hand side panel). Fires from Modis are represented as red circles whose diameter is proportional to the fire radiative power.

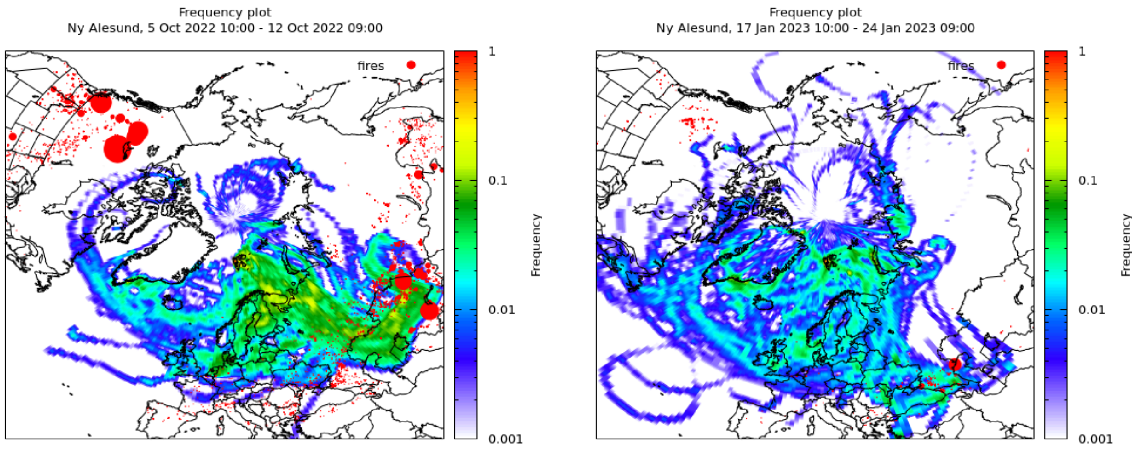

Figure S19: Frequency plot (note the logarithmic scale) for trajectories reaching the site from 10:00 of Oct 5 to 9:00 of Oct 12, 2022 (left hand side panel) and from 10:00 of 17 Jan to 9:00 24 Jan 2023 (right hand side panel). Fires from Modis are represented as red circles whose diameter is proportional to the fire radiative power.

Table S2. Percent of variance obtained by Partial Least Squares Discriminant Analysis (PLS-DA) where X represents 30 variables (compounds) and Y defines the sites classification.

Number of Factors	Variance Explained for X Effects (%)	Cumulative X Variance (%)	Variance Explained for Y Responses (%)	Cumulative Y Variance (%)
1	29.5	29.5	39.9	39.9
2	8.3	37.7	21.2	61.2
3	8.6	46.3	5.4	66.6
4	9.6	56.0	2.0	68.6
5	4.6	60.6	3.9	72.6
6	9.6	70.2	1.5	74.0
7	5.7	75.9	1.2	75.3
8	3.5	79.3	0.8	76.1
9	1.3	80.7	1.8	77.8
10	2.3	83.0	0.5	78.3
11	3.1	86.1	0.2	78.6
12	1.7	87.7	0.2	78.8
13	2.4	90.2	0.1	78.8
14	1.2	91.3	0.1	78.9
15	1.6	92.9	0.0	79.0

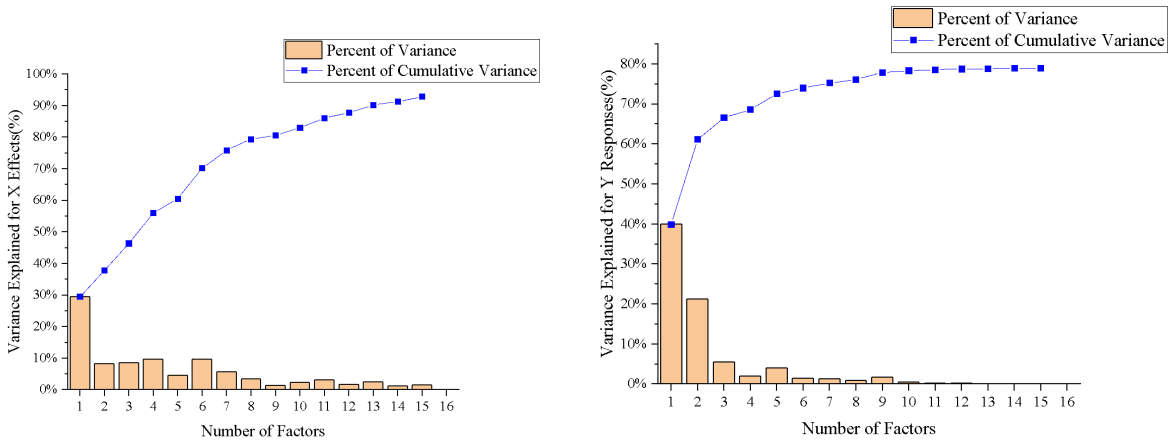

Figure S20. Percent of variance obtained by Partial Least Squares Discriminant Analysis (PLS-DA) where X represents 30 variables (compounds) and Y defines the sites classification.